ELSEVIER

Journal of Chromatography A, 672 (1994) 11–24

JOURNAL OF CHROMATOGRAPHY A

Role of local antibody density effects on immunosorbent efficiency

Anuradha Subramanian[a], Kevin E. Van Cott[a], Dean S. Milbrath[b], William H. Velander*[,a]

[a]*Department of Chemical Engineering, Virginia Tech University, Blacksburg, VA 24061, USA*
[b]*3M Bioapplications, 3M Center, St. Paul, MN 55144, USA*

(First received November 17th, 1993; revised manuscript received February 14th, 1994)

Abstract

This study evaluates the effect of immobilized antibody density on the performance of an immunosorbent. In contrast to previous studies that emphasize the correlation of high volume averaged antibody density with immunosorbent performance, we have studied the effects of locally high antibody density and spatial distribution on the antigen binding efficiency under conditions of dynamic loading and elution. The distribution of an anti-human Protein C monoclonal antibody immobilized on 3M Emphaze AB1 Biosupport Medium was evaluated. The distribution of immobilized antibody was controlled by a two-step sequence of permeation and reaction. Labeled antibody was visualized by immunofluorescence. Conditions of low pH, low temperature, and the presence of a competitor nucleophile sufficiently depressed the Thiele modulus for coupling to enable permeation of the antibody. The adsorption of the permeated antibody was enhanced by the presence of 0.75 *M* Na_2SO_4, and then the pH was raised to achieve rapid covalent coupling. Bead-averaged antibody densities of 1–11 mg/ml of hydrogel support were studied. Immunosorbents containing more evenly distributed antibody gave a two- to three-fold greater antigen binding efficiency than those with locally high antibody densities. No appreciable changes in mass transfer characteristics were observed using breakthrough analysis for immunosorbents with distributed *versus* locally high antibody density.

1. Introduction

Immunoaffinity chromatography is a process in which the binding affinity of an antigen (Ag) to a parent antibody is used as the basis for separation, where one of the species is immobilized. Monoclonal antibodies (mAbs) can be selected for a high degree of avidity for an antigen and gentle elution conditions [1–3]. While being a powerful tool for protein purification, the high cost of mAb production and low volume averaged antigen binding efficiency ($\langle \eta_{Ag} \rangle$) of immobilized mAbs makes immunoaffinity chromatography an expensive purification technique. The development of methods that increase the antigen binding efficiency can make immunosorbents more cost effective both at laboratory and industrial scales.

Antigen binding efficiency can be affected by the orientation and localized density of the immobilized antibodies [1,3]. At high localized densities the antigen binding sites of the antibodies may be in sufficient proximity to cause steric hindrance and restricted access of antigen

* Corresponding author.

0021-9673/94/$07.00
SSDI 0021-9673(94)00164-5

Table 1
Summary of immobilized antibody density effects

Reference	Support	mAb/Antigen	Density (mg/ml)	Efficiency (%)
Eveleigh and Levy [6]	Sepharose 4B	Anti-HSA/HSA	1.5	27
			22	10.5
Fowell and Chase [7]	Sepharose 4B	Anti-β-galactosidase/ β-galactosidase	0.3	5.5
			13.8	5.5
Tharakan *et al.* [8]	Sepharose CL2B	Anti-FIX/FIX	1.6	61
			9.67	17
Katoh [9]	Sepharose 4B	Anti-BSA/BSA	1	22
			30	15
Katoh [9]	Activated CH Sepharose 4B	Anti-BSA/BSA	2	18
			25	10
Katoh [9]	Formyl Cellulofine	Anti-BSA/BSA	2	30
			20	10
Strauss *et al.* [10]	CM BioGel A	Anti-FIX/FIX	0.71	20
			15.83	8
Strauss *et al.* [10]	Affi-Gel 202	Anti-FIX/FIX	0.58	28
			19.52	8

to the binding site on the antibody [3]. It also has been postulated that restricted access to the support interior can be caused by high densities of immobilized protein near the surface [4,5]. However, immunosorbent performance is usually correlated with volume-averaged antibody densities ($\langle \rho_{mAb} \rangle$, mg antibody/ml of resin or hydrogel), not local immobilized densities (ρ_{mAb}).

Many researchers have observed lower immunosorbent activity at high volume averaged antibody densities (Table 1). Antibody density effects similar to those that occur in agarose-based supports have also been reported in silica supports [11–14]. In all the immunoaffinity systems reported, the efficiency of the immobilized antibody decreased or remained constant as immobilized antibody density increased. None of the above studies distinguished between $\langle \rho_{mAb} \rangle$ and ρ_{mAb}. This work evaluates the relationship between $\langle \rho_{mAb} \rangle$, ρ_{mAb} and the performance of immunosorbents.

2. Theoretical background

Most protein immobilization on particulate supports is done in a batch mode where intraparticle diffusion is the rate-limiting mass transfer step. Modelling studies have shown that it is primarily the ratio of the reaction rate to the intraparticle diffusion rate that governs the distribution of immobilized antibody [15–18]. The Thiele modulus (Φ^2) is a dimensionless group derived from the governing equations modelling the simultaneous processes of intraparticle diffusion and reaction [15–18]. Φ^2 is of the form

$$\Phi^2 = \frac{R^2 k C}{D_{eff}} \tag{1}$$

where k is a coupling reaction rate coefficient, C is the ligand concentration, R is the radius of the bead support, and D_{eff} is the effective diffusivity of the protein in the matrix.

The distribution of immobilized mAbs within a support matrix can be controlled by changing the Thiele modulus (Φ^2) for the coupling reaction. The rate of diffusional transport of protein into the matrix is primarily determined by the characteristic length over which diffusion will occur (R^2) and by D_{eff}. For low solids content hydrogels, D_{eff} of proteins may be on the order of magnitude of that in a purely aqueous environment, essentially not affected by pH 4–9, and a weak function of temperature. Tyn and Gusek

[19] have compiled experimental values of protein diffusivities and predictive correlations of the form

$$D_{\text{eff}} = \text{f}(T, 1/M_{\text{r}}) \tag{2}$$

Once mAb is delivered to reactive sites within the support matrix, the rate of the mAb coupling can be divided into a sequence of adsorption and then covalent reaction. mAb concentration may be seen as the major driving force for the adsorption step. Previous studies have shown that increasing the adsorption of proteins onto matrices also increases the yield of immobilized protein [20–22]. We have used Na_2SO_4 to enhance adsorption of mAbs onto Emphaze AB1 and increase coupling efficiencies [20]. Once adsorbed, the rate of coupling of ligand (*i.e.*, mAb) to the reactive matrix is a strong function of pH and temperature. For example, the lysyl residues of a protein (pK_a about 10) will become markedly better nucleophiles at pH greater than about 9. Conversely, the activated (electrophilic) sites on the matrices will have an optimal pH range where competition between acid-catalyzed hydrolysis at low pH and base-catalyzed hydrolysis at high pH will compete with the coupling reaction with lysyl residues.

The functional form of the rate of the combined adsorption and coupling reaction (R_c) for protein near the reaction site can be expressed as the following:

$$R_{\text{c}} = \frac{k \cdot \text{f1}(C_{\text{mAb}} \cdot N_{\text{sites}})}{C_{\text{mAb}} + \text{f2}(N_{\text{sites}})} \tag{3}$$

$$k = k_0 \, \text{e}^{-E_{\text{act}}/RT}$$

where we view k as a strong function of pH (E_{act} is the activation energy). The number of reactive sites (N_{sites}) will strongly affect R_c. The radial profile of N_{sites} has not been well studied, but we note that the nature of many derivatization procedures may well result in a higher concentration of reactive sites near the edge of beaded supports relative to that found in the bead interior. If the functions f1 and f2 of Eq. 3 are assumed to be first order with respect to N_{sites} as described by Michaelis–Menten or Langmuir adsorption kinetics [21], then R_c can be decreased by lowering the N_{sites} available for mAb immobilization. We have achieved this by simultaneous reaction with a nucleophilic competitor such as a primary amine like Tris.

The process of immunosorption onto a support matrix can be mechanistically viewed as diffusional transport of antigen to the immobilized mAb followed by adsorption and complexation steps. A rate limitation due to mass transfer was not evidenced by the Ag breakthrough and wash profiles (Fig. 4a–d). Thus, we here emphasize the effects of ρ_{mAb} on the kinetics of Ag binding and its relationship to the pointwise antigen binding efficiency [$\eta_{\text{Ag}}(r)$] and then to the bead-average functional efficiency ($\langle \eta_{\text{Ag}} \rangle$). For clarity, we first discuss the elementary reaction steps for antigen capture by mAb in solution, and then we will extend the concept to the more complex situation of immobilized mAb. The elementary reactions steps for antigen capture by mAb in solution can be described by

$$Mab + Ag \underset{k_{r1}}{\overset{k_{f1}}{\rightleftharpoons}} [Mab \cdot Ag_1] \tag{4a}$$

$$[Mab \cdot Ag_1] + Ag \underset{k_{r2}}{\overset{k_{f2}}{\rightleftharpoons}} [Mab \cdot Ag_2] \tag{4b}$$

$$R_{\text{ic}} = R_{\text{id}} \approx 0 \tag{4c}$$

$$K_{\text{eq1}} \equiv \frac{C_{\text{mAb}\cdot\text{Ag}_1}}{C_{\text{mAb}} C_{\text{Ag}}} = \left(\frac{k_{\text{f1}}}{k_{\text{r1}}}\right)_{\text{solution}} \tag{4d}$$

$$K_{\text{eq2}} \equiv \frac{C_{\text{mAb}\cdot\text{Ag}_2}}{C_{\text{mAb}\cdot\text{Ag}_1} C_{\text{Ag}}} = \left(\frac{k_{\text{f2}}}{k_{\text{r2}}}\right)_{\text{solution}} < K_{\text{eq1}} \tag{4e}$$

The elementary reactions for filling the first antigen binding site are given by Eq. 4a. The elementary reactions for filling the second antigen binding site are given by Eq. 4b. At conditions near to that of equilibrium binding, the sum of the forward (R_{ic}) and backward (R_{id}) reactions rates for each site is approximately zero (Eq. 4c). Based upon protein structure [23], the two Ag binding sites on an empty mAb molecule are assumed to be kinetically indistinguishable. It is only when a large Ag is bound to the first site that a kinetic distinction between the first and second Ag binding site of an individual mAb molecule becomes necessary.

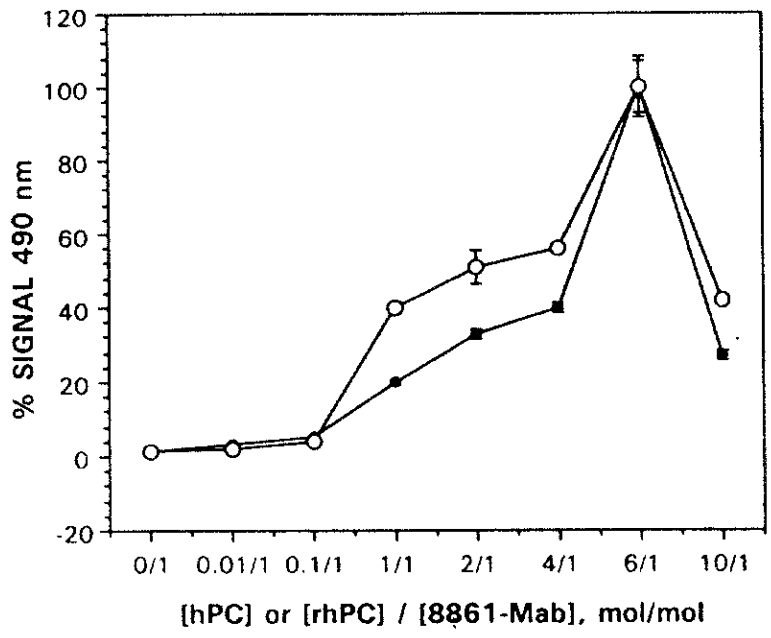

Fig. 1. Binding experiments. Increasing concentrations of (●) hPC and (○) rhPC were incubated with 8861-mAb (0.032 μM) for 1 h at 25°C, and then added to rabbit anti-hPC coated wells. After 1 h of incubation at 37°C, goat anti-mouse IgG HRP conjugate was added to the wells and incubated for 1 h. The hPC–or rhPC–8861-mAb complex was detected and quantified with OPD and reading at 490 nm.

From the solution phase experiments presented here (Fig. 1), we conclude that K_{eq2}, which describes the equilibrium filling of the second antigen binding site, is less than K_{eq1} (Eq. 4e). An increase in % ELISA (enzyme-linked immunosorbent assay) signal as a function of increasing molar concentration of either human Protein C (hPC) or recombinant hPC (rhPC) is indicative of the relative avidity of the two antigen binding domains for hPC or rhPC. Fig. 1 suggests that a large concentration driving force (corresponding to a stoichiometric ratio of Ag:mAb = 6:1) is required to overcome the decreased avidity for filling of the second Ag binding site in solution. This behavior is typical of the mAb we have studied for binding large Ags such as hPC ($M_r = 62\,000$).

The rate expressions for R_{ic} and R_{id} are functions of C_{mAb}, C_{Ag}, $C_{mAb\cdot Ag_1}$, $C_{mAb\cdot Ag_2}$, and the elementary forward (k_{f1}, k_{f2}) and backward (k_{r1}, k_{r2}) rate coefficients. For solution phase mAb–Ag reactions the equilibrium constants defined for K_{eq1} and K_{eq2} can be related to k_{f1}/k_{r1} (Eq. 4d), and k_{f2}/k_{r2} (Eq. 4e). In an analogous way, the combined forward (R_{ic}) and backward (R_{id}) reactions rates can be related to the respective K_{eq1} and K_{eq2} for Ag in equilibrium with immobilized mAb. Under conditions where Ag diffusional transport is not rate limiting, the forward rate of immunocapture (R_{ic}) of Ag by a mAb immobilized with proper orientation can be given by

$$R_{ic} = k_{f1}\rho_{mAb}C_{Ag} + k_{f2}\rho_{mAb\cdot Ag_1}C_{Ag} \tag{5a}$$

$$k_{f1} = k_{f1,0}\exp\left[-\frac{E_{act,0}\cdot f1(\rho_{mAb}, \rho_{mAb\cdot Ag_1}, \rho_{mAb\cdot Ag_2})}{RT}\right] \tag{5b}$$

$$k_{f2} = k_{f2,0}\exp\left[-\frac{E_{act,0}\cdot f2(\rho_{mAb}, \rho_{mAb\cdot Ag_1}, \rho_{mAb\cdot Ag_2})}{RT}\right] \tag{5c}$$

where a kinetic expression of the local solution phase concentration of antigen (C_{Ag}) and the local solid phase concentrations of immobilized mAb (ρ_{mAb}) and mAb–Ag complexes ($\rho_{mAb\cdot Ag_1}$, $\rho_{mAb\cdot Ag_2}$) is proposed. The expressions for the two rate constants k_{f1} and k_{f2} govern the high avidity of the first Ag binding site and the lesser relative avidity of the proximal Ag binding sites due to intra/intermolecular steric hindrance by neighboring mAbs or a sufficiently large Ag occupying that first site. Conceptually, intramolecular and intermolecular steric hindrances of the Ag binding site result in a higher activation energy in R_{ic} that is needed to "push" the antigen into a combined state with the mAb. Hence, f1 (Eq. 5b) and f2 (Eq. 5c) serve as scaling factors to increase the unhindered activation energy $E_{act,0}$ for Ag binding as ρ_{mAb}, $\rho_{mAb\cdot Ag_1}$, and $\rho_{mAb\cdot Ag_2}$ are increased. We assume that $E_{act,0}$ is the same for solution phase or immobilized mAb having proper orientation. Note that R_{ic} becomes highly dependent upon intraparticle position if ρ_{mAb} varies with position.

At equilibrium, the pointwise antigen binding efficiency $\eta_{Ag}(r)$ can be related to K_{eq1} and K_{eq2}

through $\rho_{mAb\cdot Ag_1}$, $\rho_{mAb\cdot Ag_2}$. Antigen binding efficiency $\eta_{Ag}(r)$ is defined by

$$\eta_{Ag}(r) \equiv \left[\frac{\rho_{mAb\cdot Ag_1} + \rho_{mAb\cdot Ag_2}}{\rho_{mAb}}\right]_{r=r} \cdot \frac{1\,mol\,mAb}{2\,mol\,Ag} \cdot 100\% \quad (6)$$

At conditions of equilibrium, Eq. 6 can be rewritten in terms of the defined equilibrium constants that are analogous to those given by Eqs. 4d and e, but that are now written in terms of the solid-phase concentrations of immobilized mAb and mAb–Ag complexes (ρ_{mAb}, $\rho_{mAb\cdot Ag_1}$, $\rho_{mAb\cdot Ag_2}$).

$$\eta_{Ag}(r) = [K_{eq1}C_{Ag}\{1 + K_{eq2}C_{Ag}\}]_{r=r} \cdot \frac{1\,mol\,mAb}{2\,mol\,Ag} \cdot 100\% \quad (7)$$

Note that if the functional forms of both R_{ic} and R_{id} are known, they are relatable to $\eta_{Ag}(r)$ by K_{eq1} and K_{eq2}. Finally, $\eta_{Ag}(r)$ is integrated over the whole volume of the bead (V) to give the bead-average functional efficiency ($\langle\eta_{Ag}\rangle$).

$$\langle\eta_{Ag}\rangle = \frac{\int_V \eta_{Ag}(r)\,dV}{\int_V dV} \quad (8)$$

$\langle\eta_{Ag}\rangle$ is the most commonly used measure of immunosorbent efficiency [6–10]. From Eq. 4c and Eqs. 6–8, a local increase in R_{ic} relative to R_{id} will result in an increase in $\eta_{Ag}(r)$; those mAbs with very slow R_{ic} due to locally high ρ_{mAb} will have lower $\eta_{Ag}(r)$.

3. Methods

3.1. Materials and reagents

Murine pH- and EDTA-dependent anti-human Protein C monoclonal antibodies (8861-mAb and 7D7B10-mAb) were provided by the American Red Cross (Rockville, MD, USA). Rabbit antisera against human Protein C, affinity-purified goat anti-mouse (whole molecule), and sheep anti-goat, goat anti-mouse immunoglobulins conjugated to horseradish peroxidase (HRP) were purchased from Sigma (St. Louis, MO, USA). Goat anti-human Protein C antisera was purchased from American Diagnostics (Greenwich, CT, USA). Emphaze AB1 Biosupport Medium was provided by 3M (3M Bioapplications, 3M Center, St. Paul, MN, USA). Immulon II microtiter plates were purchased from Fisher Scientific (Pittsburgh, PA, USA) hPC was provided by the American Red Cross. rhPC was isolated from transgenic porcine whey using ion-exchange and immunoaffinity chromatography [24]. JB4 histological embedding kit was purchased from Polysciences (Warrington, PA, USA). Texas red acid chloride labeled anti-mouse antisera was purchased from Vector Laboratories (Burlingame, CA, USA). *o*-Phenylenediamine–2HCl (OPD) tablets were purchased from Abbott Laboratories (Chicago, IL, USA). Immunoaffinity chromatography was performed with C_{10} columns from Pharmacia (Piscataway, NJ, USA). A Rainin data acquisition system along with a Knauer spectrophotometer was used to monitor column-mode separations. All other reagents were purchased from Sigma at the best grade available.

Emphaze AB1 ($d_p = 60\ \mu m$) is a polymer-based affinity support, synthesized by a copolymerization reaction of 2-vinyl-4,4-dimethyl-1,3-oxazolin-5-one and methylenebisacrylamide at various ratios to yield a rigid and macroporous support for bioseparations [20]. The azlactone functionality readily undergoes a ring-opening reaction with nucleophiles (ex:–NH_2 moieties on the antibody/proteins) to yield stable covalent linkages. The stability of the reactive azlactone functionality under a wide range of pH and temperature makes Emphaze AB1 Biosupport Medium a suitable support for this study.

3.2. Emphaze AB1 immunosorbent preparation

Reference coupling procedure [R] [20]

8861-mAb was incubated for 1 h at room temperature (RT) with dry azlactone beads in coupling buffer (0.05 *M* sodium phosphate–0.75 *M* Na_2SO_4, pH 7.0) containing 1–10 mg of antibody to yield 1–3 ml of immunosorbent. For target densities of 1–2 mg mAb/ml of gel a final

mAb concentration of 0.8–1.0 mg mAb/ml was used, and for target densities of 3–10 mg mAb/ml of gel, a final mAb concentration of 3 mg/ml was used. Residual reactive sites were blocked with ethanolamine. The beads were then washed with 0.5 *M* NaCl and equilibrated with loading buffer for protein immunosorption. Supernatants from all blocking and wash steps were saved for mAb determination by ELISA. The columns were analyzed for mAb leaching during chromatographic runs by ELISA.

Alternate immobilization strategy [A] (two-step method)

8861-mAb (at the same final mAb concentrations as the reference method) was incubated with dry azlactone beads at pH 4.0 for 10 min at 4°C in the presence of 0.5 *M* Tris–HCl and in the absence of Na_2SO_4 in a binary buffer system (50 m*M* acetate, 0.5 *M* Tris–HCl). At the end of the permeation step, the salt concentration was raised to 0.75 *M* Na_2SO_4 and the reaction was allowed to proceed for an additional 10 min. The pH was increased to 9.0 with 1 *M* NaOH and the reaction was allowed to proceed for another 40 min at 4°C at pH 9.0 (a total of 60 min at 4°C). The reference blocking protocol was followed. The supernatants from all blocking and wash steps were assayed for mAbs by ELISA. Columns were analyzed for mAb leaching during chromatographic runs by ELISA.

3.3. Effect of pH/competitor on coupling efficiency

Small-scale experiments (final immunosorbent volume of 40–50 μl) were conducted to determine the pH-dependent mAb coupling efficiency of Emphaze AB1 biosupport medium at 4°C. A ternary buffer system of acetate, phosphate and pyrophosphate (50 m*M* each, 0.75 *M* Na_2SO_4) was adjusted to a final pH of 4–9 with either HCl or NaOH. 7D7B10-mAb (200 μg) was suspended in the ternary buffer at the indicated pH, and dry azlactone beads were added to the reaction tubes. A target $\langle \rho_{mAb} \rangle$ of 5 mg/ml gel was used in these experiments, and the reactions were run in duplicate. To monitor the extent of reaction, the reaction was terminated at 5, 15, 30 min. Supernatant was drawn off for mAb determination by ELISA. The effect of Tris–HCl (0.1 *M*, 0.5 *M*) and salt (Na_2SO_4) on the mAb coupling efficiency at pH 4.0 was determined by similar methods. The condition leading to the slowest rate of immobilization was selected for the first step of our alternate immobilization strategy.

3.4. Chromatography

Columns (I.D. = 1 cm) were packed with approximately 1 ml of 8861/Emphaze AB1 immunosorbent, cleaned with at least 10 column volumes of 2 *M* NaSCN, and then equilibrated with at least 20 column volumes of loading buffer (20 m*M* sodium citrate, 80 m*M* sodium chloride, pH 6.5). After equilibration, pure rhPC at a concentration of 1–2 mg/ml was loaded at about 1 ml/min [linear velocity (u_o) = 1.3 cm/min] until the breakthrough front leveled off. The columns were then washed with the loading buffer until baseline was reached. Bound rhPC was eluted with either a two-step sequence of a pH 10 buffer (0.1 *M* sodium bicarbonate, 0.15 *M* sodium chloride, pH 10) and then 2 *M* NaSCN, or by a single 2 *M* NaSCN elution. All chromatographic fractions were saved for rhPC determination by ELISA.

3.5. Assays

Determination of mAb

Immulon II microtiter plates were coated with 100 μl/well of 1:200 diluted anti-mouse whole molecule in 0.1 *M* $NaHCO_3$ (pH 9.3) for 24 h at 4°C. Wells were washed with 12.5 m*M* Tris–0.05 *M* NaCl–0.05% Tween (TBS–Tween) and the residual reactive sites were blocked with TBS–0.1% BSA (TBS–BSA) for 20 min at RT. Dilutions of standard and samples in TBS–BSA were added to the wells and incubated for 20 min at 37°C. After incubation wells were washed and 1:1000 diluted HRP-conjugated goat anti-mouse IgG was added to the wells and incubated for 20 min at 37°C. Wells were washed and OPD substrate was added to each well. The colorimet-

ric reaction was stopped after 3 min by the addition of 1.5 *M* H_2SO_4 to each well. The plates were read at 490 nm using an EL308 Bio-Tek Microplate reader. The amount of antibody immobilized on the support matrix and the amount of antibody leaching were evaluated by this assay.

Determination of Protein C by polyclonal ELISA

Immulon II plates were coated overnight with 100 μl/well of 5 μg/ml of rabbit anti-human Protein C in 0.1 *M* $NaHCO_3$, pH 9.3 at 4°C. Wells were washed with TBS–Tween. 100 μl of standard and samples in the dilution buffer (TBS–0.1% BSA, pH 7.0) was added to all the wells and incubated at 37°C for 20 min. Wells were washed four times and the bound PC was detected by a sandwich of goat anti-human protein C and HRP-conjugated sheep anti-goat IgG. The plates were read at 490 nm.

Binding experiments

Immulon II plates were coated overnight with 100 μl/well of 5 μg/ml of rabbit anti-human Protein C in 0.1 *M* $NaHCO_3$, pH 9.3 at 4°C. The wells were then washed with TBS–Tween and residual reactive sites were blocked with TBS–BSA for 15 min at RT. Solutions of 0.032 μM 8861-mAb (final concentration) with increasing amounts of hPC or rhPC ranging from 0.04 to 0.32 μM (final concentration) were pre-equilibrated for 1 h at 25°C, and 100 μl of the mAb/hPC or rhPC mixture were added to the IgG-coated wells and incubated at 37°C for 1 h. After washing with TBS–Tween, 100 μl of 1:1000 diluted HRP-conjugated goat anti-mouse IgG was added to the wells. After a 1 h incubation and washing, OPD was added to each well, the reaction was quenched with 1.5 *M* H_2SO_4 after 3 min, and the plate was read at 490 nm.

Immunofluorescent staining of Emphaze AB1 beads

The distribution of mAb in azlactone beads at various densities was determined immunofluorescent microscopy. Texas Red labeled anti-murine IgG (whole molecule) was bound to azlactone beads by the reference as well as two-step procedures at targeted densities of 1, 3 and 8 mg mAb/ml of hydrogel. Dehydrated beads were infiltrated and embedded in JB-4 embedding resin according to manufacturer's instructions. Cross-sections, 10 μm thick, were cut from the block using an LKB automatic microtome. Fluorescent photomicrographs were taken using Kodak Ektar 1000 film.

4. Results

4.1. Binding experiments

The binding of divalent Fab domains on 8861-mAb to hPC (from human plasma) or rhPC was evaluated by ELISA. Fig. 1 presents the ELISA signal resulting from the immunocapture of the (r)hPC–8861-mAb complex formed in solution. Each sample was run in triplicate, error bars are imperceptible for some data. A low and relatively constant response resulted at molar Ag:mAb ratios up to 0.1:1 for both hPC and rhPC. The signal then gradually increased for both rhPC and hPC for molar Ag:mAb ratios from 1:1 to 4:1. A sharp maximum in absorbance was observed at an Ag:mAb ratio of 6:1. rhPC was used for our studies because of the availability of rhPC and the similar avidity of 8861-mAb to hPC and rhPC.

4.2. Effect of pH/competitor on coupling kinetics

To gain a better understanding of the impact of surface density of immobilized mAb on the functional efficiency, we have developed an immobilization strategy to yield a uniform distribution of mAbs throughout the bead cross-section. The distribution of mAbs within the porous support was achieved by controlling both the Thiele modulus for mAb immobilization and by simultaneous titration of reactive sites with a nucleophilic competitor (Tris).

The effect of pH on mAb coupling efficiency (total mAb immobilized/total mAb input) for small-scale columns (40–50 μl) is shown in Fig.

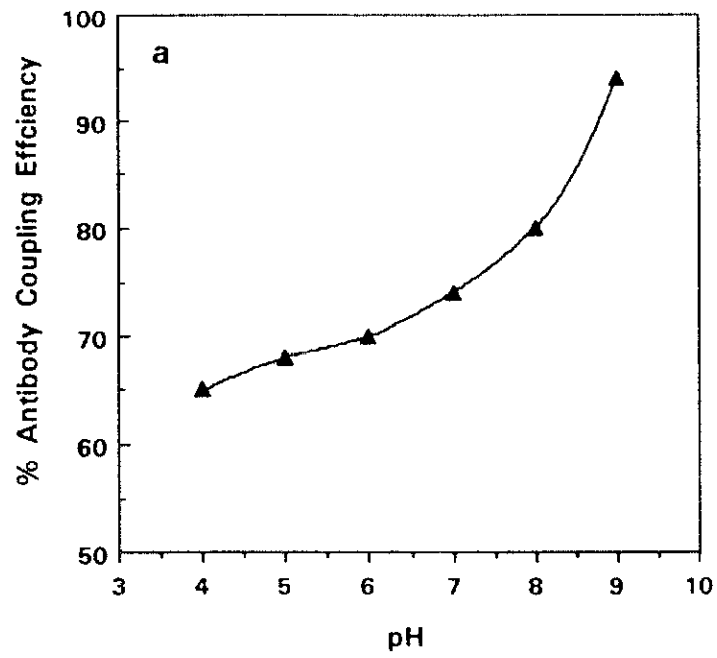

Fig. 2. (a) Effect of coupling pH on mAb immobilization efficiency. Murine EDTA dependent anti-hPC mAb (7D7B10-mAb) was incubated in a ternary buffer (50 m*M* acetate, phosphate, and pyrophosphate) with 0.75 *M* Na_2SO_4 for 30 min at pH 4, 5, 6, 7, 8, 9. Immobilizations were performed as outlined in the Methods section. mAb in feed and coupling step supernatants was assayed by ELISA described in Methods. mAb coupling efficiency is defined as the ratio of total mAb bound to the total mAb input. (b) Effect of salts/Tris on mAb immobilization efficiency. Murine EDTA dependent anti-hPC mAb (7D7B10-mAb) was incubated in 50 m*M* acetate buffer (pH 4.0) both in the presence and absence of 0.75 *M* Na_2SO_4. Immobilizations were performed in the presence of 0.1 or 0.5 *M* Tris–HCl as outlined in the Methods section. mAb coupling efficiency is calculated as in Fig. 3a. Case 1: 0.1 *M* Tris–0.75 *M* Na_2SO_4, 4°C. Case 2: 0.5 *M* Tris–0.75 *M* Na_2SO_4, 4°C. Case 3: 0.1 *M* Tris–0.0 *M* Na_2SO_4, 4°C. Case 4: 0.5 *M* Tris–0.0 *M* Na_2SO_4, 4°C. Case 5: 0.05 *M* sodium phosphate–0.75 *M* Na_2SO_4/pH 7.0, RT.

2a. Immobilization of 7D7B10-mAb at pH 4.0 yielded a mAb coupling efficiency of 65% with a $\langle \rho_{mAb} \rangle$ of 3.2 mg/ml. mAb coupling efficiency increased with pH, with an efficiency of 95% obtained at pH 9.0 to yield a $\langle \rho_{mAb} \rangle$ of 4.8 mg/ml of gel.

The effect of salts, nucleophilic competitor species (*i.e.*, Tris), and temperature on mAb coupling efficiency is shown in Fig. 2b. A target mAb density of 5 mg/ml was used in these experiments. mAb immobilized at pH 7.0 (0.75 *M* Na_2SO_4, no Tris) at RT for 15 min resulted in an average mAb coupling efficiency of 95% (Case 5). Immobilization of mAbs at pH 4 in the presence of 0.75 *M* Na_2SO_4 with Tris at 0.1 *M* and 0.5 *M* gave average mAb coupling efficiencies of 64% (Case 1) and 37% (Case 2), respectively. Upon elimination of Na_2SO_4, coupling at pH 4 and in the presence of 0.1 *M* Tris and 0.5 *M* Tris yielded average mAb coupling efficiencies of 54% (Case 3) and 26% (Case 4), respectively. mAbs incubated at pH 4.0, 0.5 *M* Tris, 4°C for 10 min in the absence of Na_2SO_4, followed by incubation in 0.75 *M* Na_2SO_4 for 10 min and a step change to pH 9.0 at 4°C gave a coupling efficiency of 90% with a $\langle \rho_{mAb} \rangle$ of 4.3 mg/ml.

Table 2
8861-mAb coupling efficiencies

Target density (mg/ml gel)	Actual density (mg/ml gel)	Coupling effiency (%)
Two-step coupling		
1.1	0.9	82
4.5	3.2	71
10	5.7	57
20	9.3	47
Reference coupling		
1.1	1.1	100
2.3	2.2	96
12	11.8	98

Emphaze AB1 immunosorbents were prepared by both reference and two-step methods as described in the Methods section. mAb coupling efficiency was determined as a ratio of the total mAb bound to total mAb challenge.

4.3. Analysis of coupling efficiencies

Table 2 summarizes the mAb coupling efficiencies obtained for larger columns (1–3 ml) with the alternate immobilization (A) and the reference protocol (R) recommended by the manufacturer. The immunosorbents prepared with both methods at similar target $\langle \rho_{mAb} \rangle$ were challenged with the same solution concentration of mAb. Incubation with lower concentrations of mAb ($\langle$0.1 mg/ml) at the same total mAb challenge gave lower coupling efficiencies (data not shown).

Using the reference protocol (R), 8861-mAb was immobilized at mAb densities (mg mAb/ml of hydrogel) ranging from about 1–12 mg mAb/ml of gel. A coupling efficiency of about 100% was obtained for a density of 1.1 mg 8861-mAb/ml of hydrogel. Coupling efficiencies of 96% and 98% were obtained for 8861-mAb immobilized at 2.2 and 11.8 mg/ml of hydrogel, respectively (Table 2).

Immunosorbents were prepared using the two-step procedure (A) with targeted mAb densities of 1–20 mg/ml. A coupling efficiency of 90% was achieved at mAb density of 1.0 mg/ml of hydrogel. However, at higher targeted mAb densities lower coupling efficiencies were obtained. Coupling efficiencies of 71, 57 and 47% were obtained for targeted mAb densities of 4.5, 10, 20 mg mAb/ml of hydrogel, respectively (Table 2).

Leaching of mAbs from the immunosorbents prepared by both the reference and two-step procedures was measured by mAb ELISA on the elution fractions from the first two chromatographic runs. Both A- and R-type columns (for all columns having about 1–12 mg mAb/ml support) gave a similar leaching of mAb; less than about 0.8 μg mAb per mg of rhPC was found in 2 *M* NaSCN eluates where rhPC was loaded at about 50% of theoretical capacity of the column.

4.4. Immunofluorescent staining results

Texas Red labeled antibodies were immobilized according to reference (R) and alternate immobilization procedures (A) at targeted $\langle \rho_{mAb} \rangle$ of 1–8 mg/ml, respectively. Photomicrographs of 10 μm thick bead cross-sections with mAb density of 5–6 mg/ml using fluorescent microscopy are shown in Fig. 3a and b. Beads made with the reference procedure (R) gave a shell-like profile of fluorescent signal in the outer 10 μm of the bead radii (Fig. 3a). Beads made with the alternate procedure (A) gave a more even distribution of the fluorescent signal throughout the cross section (Fig. 3b).

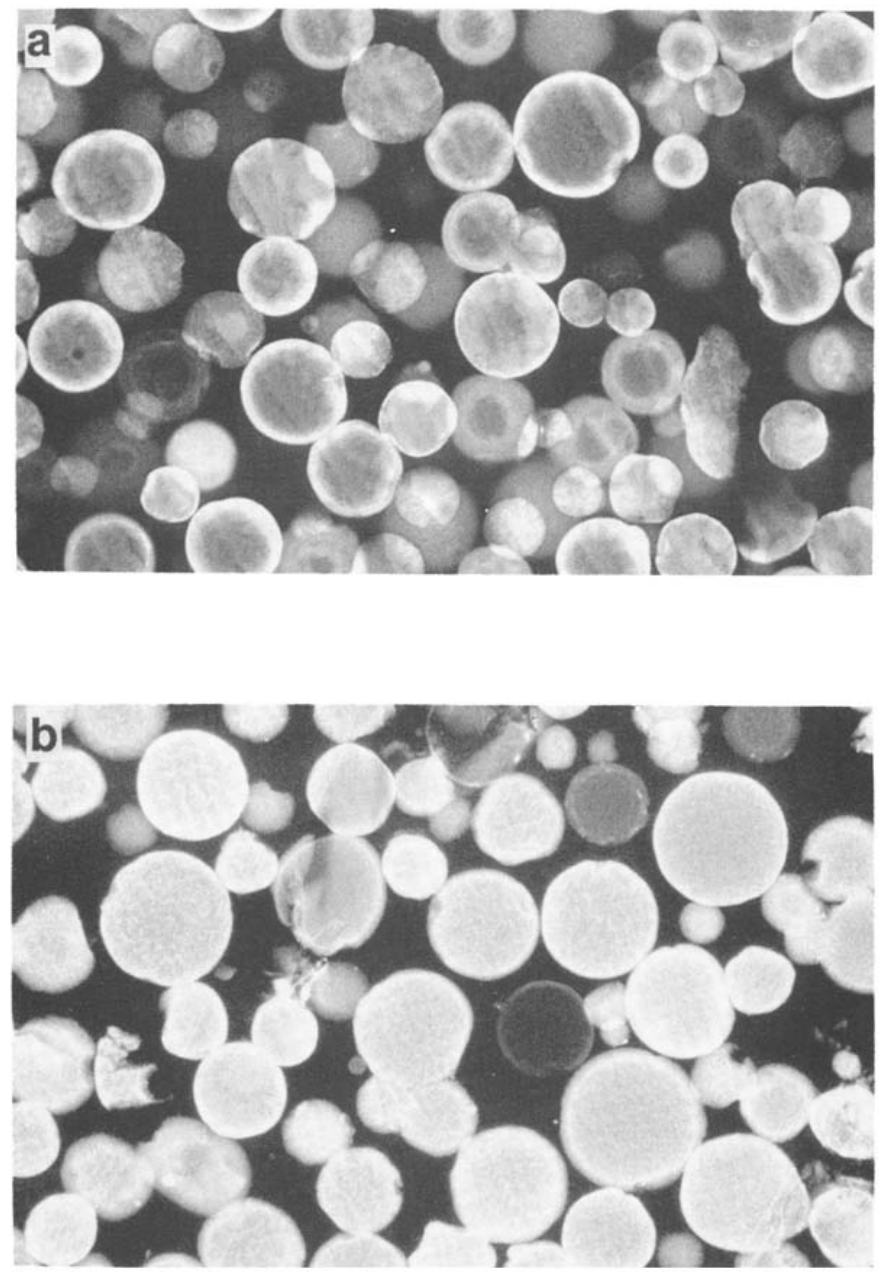

Fig. 3. Texas Red labeled beads. Texas Red labeled anti-mouse IgG was reacted with Emphaze AB1 by the reference and two-step procedures. Fluorescently labeled beads were sectioned as detailed in Methods section and viewed under fluorescent light. Panel a presents an immunosorbent prepared via the reference method at a $\langle \rho_{mAb} \rangle$ of 6.0 mg/ml. Panel b presents an immunosorbent prepared via the alternate immobilization strategy (two-step method) at a $\langle \rho_{mAb} \rangle$ of 5.5 mg/ml.

Table 3
Performance of immunosorbents under breakthrough loading

mAb density (mg/ml)	Run No.	CV[a] (ml)	Flow-rate (ml/min)	Ag loaded (mg)	PC eluted (μg)	Efficiency (η_{Ag}) (%)
Two-step coupling						
0.9	1	1.0	1.0	11	156	22
	2	0.86	0.86	8.0	141	23
3.2	1	1.0	1.0	12	1407	55
	2	1.0	1.0	30	1595	62
9.3	1	1.0	1.0	28	4891	65
	2	1.0	1.0	50	4402	59
Reference coupling						
1.1	1	1.0	1.0	21	180	20
	2	1.0	1.0	8.0	234	26
2.2	1	0.86	0.86	35	471	31
	2	0.86	0.86	12	429	28
11.8	1	1.0	1.0	28	2092	22
	2	1.0	1.0	50	2700	28

Emphaze AB1 immunosorbents described in Table 2 were challenged with pure rhPC in 20 m*M* sodium citrate, 80 m*M* NaCl, pH 6.5. The concentration of rhPC in the feed ranged from 1–2 mg/ml. In each experiment columns with $<\rho_{mAb}>$ of 0.9 (A) and 1.1 (R) mg/ml columns were loaded with 10 CVs of feed, 3.2 (A) and 2.2 (R) mg/ml columns were loaded with 15 CV of feed, and 9.3 (A) and 11.8 (R) mg/ml columns were loaded with 25 CVs of feed. Antigen was eluted from the column by a pH 10 elution (0.1 *M* $NaHCO_3$, 0.15 *M* NaCl, pH 10) followed by a 2 *M* NaSCN elution, the two elution fractions being summed to give the total rhPC eluted. The elution fractions were analyzed by ELISA. Antigen binding efficiency of immunosorbents is defined as the percent of the theoretical maximum binding capacity, assuming a 2:1 antigen to antibody stoichiometry.

[a] CV = Column volume.

4.5. Breakthrough analysis

Table 3 gives operating conditions and antigen binding efficiencies obtained from breakthrough experiments. The antigen-binding efficiencies were calculated using the total amount of rhPC eluted from the sequence of pH 10 and 2 *M* NaSCN elutions. Since the 8861-mAb is an IgG-2A class immunoglobulin, antigen binding efficiency ($\langle\eta_{Ag}\rangle$) of the immobilized mAb was calculated by assuming a binding stoichiometry of two Ags per immobilized mAb. Average antigen-binding efficiencies of 23, 30 and 25% were obtained for 1.1 (R), 2.2 (R), and 11.8 (R) mg/ml columns, respectively. Average antigen-binding efficiencies of 23, 59 and 62% were obtained for 0.9 (A), 3.2 (A), and 9.3 (A) mg mAb/ml of support, respectively.

Fig. 4 shows typical breakthrough and elution profiles at 280 nm for rhPC loaded on 8861-mAb immunosorbent columns made by either reference (R) or two-step (A) methods. The shapes of the breakthrough profiles and respective 2 *M* NaSCN eluate profiles were similar for immunosorbents having comparable $\langle\rho_{mAb}\rangle$. The NaSCN product eluates spanned about 2 column volumes for the 0.9 (A) and 1.1 (R) mg/ml columns. The NaSCN product eluates spanned about 4 column volumes for the 9.3 (A) and 11.8 (R) mg/ml columns, with the two-step column (9.3 mg/ml) having about a three-fold higher binding efficiency, as determined by ELISA.

5. Discussion

In general, Φ^2 is much greater than 1 for most protein immobilization procedures [25], and thus the rate of coupling is much faster than the rate at which protein is delivered into and transported throughout the bead. For example, in the absence of a competitor nucleophile, a shell of

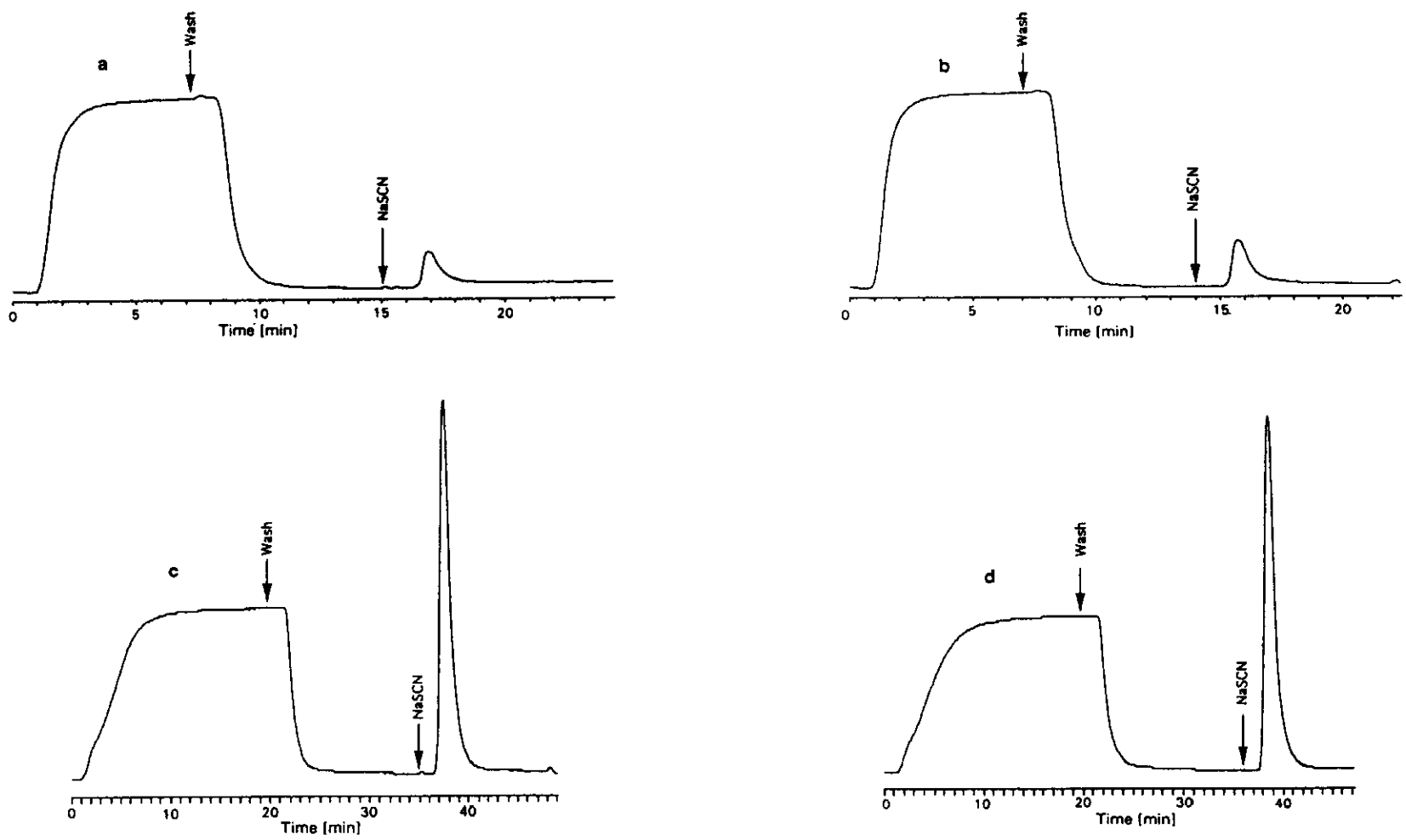

Fig. 4. Breakthrough loading of pure rhPC on Emphaze AB1 immunosorbents. Columns (I.D. = 1 cm) were packed with immunosorbents referred to in Table 2 and loaded with pure rhPC at 1 ml/min. After washing, rhPC was eluted with 2 *M* NaSCN. (a) Two-step procedure, $\langle \rho_{mAb} \rangle = 0.9$ mg/ml, flow-rate = 1 ml/min, column volume = 0.86 ml, $C_{Ag} = 1.1$ mg/ml. (b) Reference procedure, $\langle \rho_{mAb} \rangle = 1.1$ mg/ml, flow-rate = 1 ml/min, column volume = 0.79 ml, $C_{Ag} = 1.1$ mg/ml. (c) Two-step procedure, $\langle \rho_{mAb} \rangle = 9.3$ mg/ml, flow-rate = 1 ml/min, column volume = 1 ml, $C_{Ag} = 1.0$ mg/ml. (d) Reference procedure, $\langle \rho_{mAb} \rangle = 11.8$ mg/ml, flow-rate = 1 ml/min, column volume = 1.2 ml, $C_{Ag} = 1.0$ mg/ml. The amount of rhPC eluted was determined by ELISA

high density, fluorescently labeled mAb results at immobilization conditions of $\Phi^2 > 1$ (Fig. 3a). This is in part due to the high N_{sites} that occurs on Emphaze AB1 [0.25 meq/g of Emphaze AB1 (technical data on 3M Emphaze AB1 from 3M Corporation)] as well as in many other activated supports. In the case of Emphaze AB1 as well as several other activated supports (data for other supports not shown), we have found that the simultaneous conditions of low pH, low temperature and the presence of a competitor nucleophile greatly lower the coupling efficiency and enable permeation. In this work we did not directly determine if pore blockage by anchored antibody occurs at fast reaction/slow permeation conditions, or if there is just such an excess of sites to react that no antibody remains to diffuse in. However, mAb coupling yields for the reference method were greater than 96% for loadings up to about 12 mg/ml. This indicates that pore blockage at the outer edge of the support by antibodies does not occur. Rather a great excess of sites is present and thus antibody is reacted to completion before it can penetrate by diffusion.

Increased permeation was seen in the more evenly distributed fluorescently labeled mAb that was immobilized and visualized in bead cross-sections (Fig. 3b). We conclude that conditions of $\Phi^2 \langle 1$ were achieved by the low pH conditions and presence of Tris. We note that coupling efficiencies of about 40–60% still resulted at pH 4. The addition of 0.5 *M* Tris reduced the coupling efficiency to about 20–30% at pH 4. While both Tris and the lysyl residues are much less nucleophilic at lower pH, some reaction still occurs, probably by an acid-catalyzed mechanism. The Tris effectively inactivates those sites which would be likely to react with

the protein. We note that while the amine group of Tris and lysine would both be fully protonated at low pH, Tris is a very small molecule and thus "kinetically" more nucleophilic species (via acid catalyzed mechanism) than a lysyl residue tied to a large and less mobile protein molecule. Thus, Tris will be more likely to terminate a given site under acid catalyzed mechanism than a lysyl residue on a protein. We here used Na_2SO_4 to assure adsorption after permeation, and a shift to conditions of rapid reaction gave coupling efficiencies of 60–80% for $\langle \rho_{mAb} \rangle$ equal to about 6 mg/ml or less (Table 2). For the 1–6 mg/ml support mAb loadings, the combined levels of mAb and Tris were still probably less than N_{sites}. However, less than 50% yields were obtained at $\langle \rho_{mAb} \rangle$ of about 9 mg/ml, and therefore the combined levels of mAb and Tris were on the order of N_{sites}. For practical applications, the Tris concentration may need to be optimized to achieve a balance between ρ_{mAb} and higher coupling efficiencies at high $\langle \rho_{mAb} \rangle$.

Because $\langle \eta_{Ag} \rangle$ can be related to kinetic phenomena described by R_{ic} and R_{id}, both the reference and two-step immunosorbents were exposed to similar Ag concentration driving forces in each set of Ag breakthrough experiments. The steep return to baseline absorbance during the wash step of these breakthrough experiments supports our assumption that the Ag binding reactions are essentially irreversible. We have purposefully chosen 2 *M* NaSCN elution conditions for the chromatograms in Fig. 4 to elicit fast desorption kinetics and make R_{id} very large relative to R_{ic}. Past studies with 8861 immunosorbents used a pH 10 elution step [24,26]. These previous studies at pH 10 resulted in broad and tailing peaks, which is indicative of conditions where R_{id} is a rate-limiting process relative to mass transfer. It is noted that shell-type and distributed forms of immobilization at similar $\langle \rho_{mAb} \rangle$ yield similar elution profiles at given loading and elution conditions (Fig. 4), although the characteristic length needed to permeate all mAb sites with Ag is much different (Fig. 3a and b). Furthermore, the narrow peak widths obtained using NaSCN as an eluate indicate that any increased penetration needed to access interior mAb sites does not affect the Ag mass transfer rate within a high $\langle \rho_{mAb} \rangle$ immunosorbent. It appears that the amount of mAb which leaches into the 2 *M* NaSCN eluates is similar in either A or R reaction methods. This indicates that the percentage of covalently attached and physiosorbed mAb is similar for either R or A type immobilizations.

Our method of immobilization has enabled study of the relationship between $\langle \rho_{mAb} \rangle$ and ρ_{mAb} to $\langle \eta_{Ag} \rangle$. High $\langle \rho_{mAb} \rangle$ immunosorbents prepared by the reference method have two- to three-fold lower values of $\langle \eta_{Ag} \rangle$ than the two-step method (Table 3). This behavior was found over a range of $\langle \rho_{mAb} \rangle$ from about 3 to 11 mg mAb/ml support, but not for $\langle \rho_{mAb} \rangle$ less than 3 mg mAb/ml. We note that the highest combined levels of C_{mAb} and N_{sites} occur near the edge for both the reference and two-step methods during the initial contacting of the mAb with the matrix. Thus, we expect that significant reaction may occur even at bead average conditions of $\Phi^2 \langle 1$ to form locally high ρ_{mAb} at the outer edge of the beads ($r = R$). Coupling yields of about 20–30% after the first step of the two-step method (at bead average conditions of $\Phi^2 \langle 1$) probably represent mAb that has coupled near the edge at high ρ_{mAb}. The similar appearance of fluorescent-photomicrographs of bead cross sections of the two-step or reference immunosorbents at a labeled $\langle \rho_{mAb} \rangle$ of less than 3 mg mAb/ml supports this conclusion for most mAb coupled at about $r = R$. These analyses showed a narrow band of similar fluorescent signal near the edge of the bead cross-sections for two-step and reference methods (data not shown). In terms of Eqs. 4c and 5a–c, the ρ_{mAb} at about $r = R$ is sufficiently high to reduce the ratio of R_{ic} to R_{id} at that radial position.

Congruently, the two- to three-fold higher $\langle \eta_{Ag} \rangle$ found at about 3 mg/ml or greater in two-step relative to reference immunosorbents is consistent with the locally lower ρ_{mAb} at $r \langle R$, as evidenced by the more evenly distributed fluorescent signal seen in Fig. 3B. Thus, the lower $\langle \eta_{Ag} \rangle$ seen for reference relative to two-

step immunosorbents at ρ_{mAb} greater than about 3 mg/ml is kinetically consistent with a lower ratio of R_{ic} to R_{id} for a large percentage of the immobilized mAb. In summary, it is primarily the mAb immobilized away from the surface by the two-step method at $\langle \rho_{mAb} \rangle$ greater than about 3 mg/ml that benefit from higher $\langle \eta_{Ag} \rangle$ due to locally lower ρ_{mAb}.

This present work establishes the highly non-uniform distribution of mAbs and $\eta_{Ag}(r)$ in immunosorbents, and thus the oversimplifications in previous modelling studies presenting the effects of mass transfer and sorption kinetics on intraparticle concentration profiles of bound Ags [27]. Due to the high values of $\langle \eta_{Ag} \rangle$ we have achieved with our two-step method ($>50\%$), we have proposed a bivalent kinetic model for mAb–Ag interactions (Eq. 5a), rather than the traditional univalent Langmuir model presented in most modelling studies [27]. A more detailed evaluation of kinetic and mass transport effects using similar but more specific functional forms for R_{ic} (Eqs. 5a–c) and R_{id} (not given) is beyond the scope of this work, but is currently being studied to gain further insight into the role of mAb coupling on immunosorbent performance.

6. Conclusions

In the above discussion, we have hypothesized that intermolecular steric hindrance of Ag-combining sites of immobilized mAb by other proximally immobilized mAb and associated Ag–mAb complexes exists and is superimposed upon the inherent intramolecular steric hindrance by bound Ag. The local mAb density in an immunosorbent is a more critical parameter than bead-average mAb density in immunoaffinity chromatography. mAb coupling methods with a large Thiele modulus during permeation will likely result in a shell-type profile with high localized densities. Using a two-step strategy, where the Thiele modulus is low during the permeation step, a more even distribution of immobilized mAb can be achieved at high $\langle \rho_{mAb} \rangle$. This modified coupling method results in increased binding efficiency at high $\langle \rho_{mAb} \rangle$, increasing the overall usefulness of the resulting immunosorbent. The improvement is not strongly related to nor results in mass transfer restrictions in the 60 μm diameter beads studied, and thus is related to changes in the kinetics of Ag adsorption.

7. Acknowledgements

This work was supported by NSF grant BCS-9011098 AMD-2. K.E.V.C. was supported in part by the DuPont PhD Fellowship. The technical assistance of K. Hess and T. Moore is greatly appreciated. The gift of 8861-mAb and 8861-mAb immunopurified hPC from the ARC is greatly appreciated.

8. References

[1] H.A. Chase, *Chem. Eng. Sci.*, 39 (1984) 1099.
[2] C.L. Orthner, R.D. Madurawe, W.H. Velander, W.N. Drohan, F.D. Battey and D.K. Strickland, *J. Biol. Chem.*, 264 (1989) 18781.
[3] W.H. Velander, A. Subramanian, R.D. Madurawe and C.L. Orthner, *Biotechnol. Bioeng.*, 39 (1992) 1013.
[4] K.E. Dennis, D.S. Clark, J.E. Bailey, Y.K. Cho and Y.H. Park, *Biotechnol. Bioeng.*, 26 (1984) 892.
[5] Md.M. Hossain and D.D. Do, *Chem. Eng. J.*, 34 (1987) B35.
[6] J.W. Eveleigh and D.E. Levy, *J. Solid-Phase Biochem.*, 2 (1977) 45.
[7] S.L. Fowell and H.A. Chase, *J. Biotechnol.*, 4 (1986) 1.
[8] J.P. Tharakan, D.B. Clark and W.N. Drohan, *J. Chromatogr.*, 522 (1990) 153.
[9] S. Katoh, *Trends Biotechnol.*, 5 (1987) 328.
[10] W.M. Strauss, G.J. Broze, J.P. Miletich and H.R. Null, *Biotechnol. Appl. Biochem.*, 9 (1987) 462.
[11] P.D. Weston and R. Scorer, *Affinity Chromatogr.*, (1978) 207.
[12] S.R. Narayanan and L.J. Crane, *Trends Biotechnol.*, 8 (1990) 12.
[13] J.R. Sportsman and G.S. Wilson, *Anal. Chem.*, 52 (1980) 2013.
[14] D. Wu and R.R. Walters, *J. Chromatogr.*, 458 (1988) 169.
[15] D.D. Do and J.E. Bailey, *Chem. Eng. Commun.*, 12 (1981) 221.

[16] R. Scharer, Md.M. Hossain and D.D. Do, *Biotechnol. Bioeng.*, 39 (1992) 679.
[17] Md.M. Hossain, D.D. Do and J.E. Bailey, *AIChE J.*, 32 (1986) 1088.
[18] D.D. Do, D.S. Clark and J.E. Bailey, *Biotechnol. Bioeng.*, 24 (1982) 1527.
[19] M.T. Tyn and T.W. Gusek, *Biotechnol. Bioeng.*, 35 (1990) 327.
[20] P.L. Coleman, M.M. Walker, D.S. Milbrath, D.M. Stauffer, J.K. Rasmussen, L.R. Krepski and S.M. Heilmann, *J. Chromatogr.*, 512 (1990) 345.
[21] J.B. Wheatley and D.E. Schmidt, Jr., *J. Chromatogr.*, 644 (1993) 11.
[22] P.L. Coleman, M.W. Walker and D.S. Milbrath, *US Pat.*, 5 200 471, April 6, 1993.
[23] P.M. Alzari, M.-B. Lascombe and R.J. Poljak, *Ann. Rev. Immunol.*, 6 (1988) 555.
[24] T. Morcol, R.M. Akers, J.L. Johnson, F.C. Gwazdauskas, J. Knight, H. Lubon, W.N. Drohan and W.H. Velander, *Ann. N.Y. Acad. Sci.*, 721 (1994) 218.
[25] A. Borchert and K. Buchholz, *Biotechnol. Bioeng.*, 26 (1984) 727.
[26] K. Kang, D. Ryu, W.N. Drohan and C.L. Orthner, *Biotechnol. Bioeng.*, 39 (1992) 1086.
[27] M.A. McCoy and A.I. Liapis, *J. Chromatogr.*, 548 (1991) 25.